The collision-free photochemistry of methyl azide at 157 nm: Mechanism and energy release

Alfredo Quinto-Hernandez, , Shih-Huang Lee, and , and Alec M. Wodtke

---

The collision-free photochemistry of methyl azide at 157 nm: Mechanism and energy release

Alfredo Quinto-Hernandez,[1,a)] Shih-Huang Lee,[2] and Alec M. Wodtke[3,4]

[1]*National Institute of Technology of Mexico, Calzada Tecnologico 27, Zacatepec, Morelos 62780, Mexico*
[2]*National Synchrotron Radiation Research Center, 101 Hsin-Ann Road, Hsinchu Science Park, Hsinchu 30076, Taiwan*
[3]*Institut für Physikalische Chemie, Universität Göttingen, Tammannstrasse 6, D-37077 Göttingen, Germany*
[4]*Max-Planck-Institut für Biophysikalische Chemie, Karl Friedrich-Bonhoeffer-Institut, Am Fassberg 11, 37077 Göttingen, Germany*

Synchrotron radiation VUV-photoionization based photofragment translational spectroscopy was used to identify the primary and secondary photodissociation reactions of methyl azide (CH_3N_3) at 157 nm under collision-free conditions. Two primary dissociation channels are identified, leading to CH_3 + N_3 (the radical channel) and CH_3N + N_2 (the molecular elimination channel). The last channel is the major dissociation pathway, but unlike work at longer photolysis wavelengths, here, the radical channel exclusively produces the higher energy isomer cyclic-N_3. Product time-of-flight data for both channels were obtained and compared with earlier work on methyl azide photochemistry at 193 nm based on electron impact ionization, allowing us to estimate a product branching ratio $\frac{\Phi_{CH_3-N_3}}{\Phi_{CH_3-N_2}} = \frac{2.3\% \pm 0.6\%}{97.7\% \pm 0.6\%}$. *Published by AIP Publishing.* [http://dx.doi.org/10.1063/1.4997783]

INTRODUCTION

The surprising discovery of cyclic-N_3 formation in the UV photochemistry of simple azides[1,2] provides motivation to extend our understanding of azide photochemistry. Interest in cyclic-N_3 derives from the fact that observations of cyclic N-allotropes[3,4] are so rare. Moreover, new poly-nitrogen molecules might be produced using cyclic-N_3 as a precursor; for example, the formation of T_d-N_4, tetra-azatetrahedrane[5,6] is expected to occur when $N(^2D)$ reacts in the presence of cyclic-N_3 in a barrierless exothermic recombination reaction. Due to their metastability, these poly-Nitrogen molecules may decompose into environmentally clean N_2 with large exoergicity.[7,8] Hence, they are considered a novel class of high energy density materials (HEDM).[5] Cyclic-N_3 also offers the opportunity to study the effect of the geometric phase on the molecular dynamics.[8,9] High resolution IR spectra would be a remarkable test of theoretical methods in the vicinity of conical intersections.

The first experimental report of cyclic-N_3 was obtained from studies of the photodissociation dynamics of chlorine azide (ClN_3) near 235 nm using the velocity map imaging (VMI) technique.[1] This observation stimulated other investigations on ClN_3, including photofragment translational spectroscopy (PTS) experiments based on electron impact ionization (EI)[2,10,11] and synchrotron radiation VUV-photoionization[12,13] as well as extending the range of photolysis wavelengths (234-280 nm) used in additional VMI studies.[14] All these experiments were consistent with the

theoretical work[9,15] and revealed that cyclic-N_3 is a primary (collision free) product in the UV photochemistry of ClN_3. Other photochemical precursors to cyclic-N_3 have also been found. Rydberg H-atom time-of-flight studies of hydrazoic acid (HN_3) photolysis suggest cyclic-N_3 formation,[16,17] and clear evidence is found in the near threshold VUV photoionization-based PTS measurements on methyl azide (CH_3N_3) photodissociation at 193 nm.[18] A complete review is available.[19]

Due to both its energetics and dynamics, methyl azide is a potentially interesting precursor for cyclic-N_3. Cyclic-N_3 lies at about 30 kcal/mol higher in energy than the better known linear azide radical and exists behind modest barriers to dissociation (33 kcal/mol) and linearization (32 kcal/mol).[9] In any photochemical precursor, higher photolysis energy is needed to produce cyclic-N_3, while its dissociation and linearization energies are rather low. The high C–N bond energy in methylazide in comparison to the Cl–N bond energy in chlorine azide leads to lower internal energies in the azide photofragments produced by methylazide photolysis. Furthermore, in contrast to Cl, CH_3 has the potential to carry away excess energy as internal energy, potentially stabilizing the fragile cyclic product. It is with these ideas in mind that we began work on methyl azide photochemistry.

Previous work shows that there are two primary photodissociation channels in methyl azide photochemistry,

$$CH_3N_3 \rightarrow CH_3 + N_3. \tag{1}$$

$$CH_3N_3 \rightarrow CH_3N + N_2, \tag{2}$$
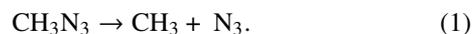
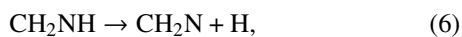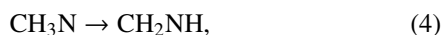where reaction (1) is commonly referred to as the radical channel and reaction (2) as the molecular elimination channel.

a)Author to whom correspondence should be addressed: alfredo.qh@itzacatepec.edu.mx

An early study on the photolysis of methyl azide at 248 nm revealed products only from the molecular channel.[20] Later, using a 193-nm radiation, a C–N bond cleavage was observed,[18] but due to the use of VUV photoionization based product detection, it was difficult to derive a reliable branching ratio since the relevant photoionization cross sections were not known. More recently, we have observed both reaction pathways in the 193-nm photolysis of CH_3N_3 using PTS with EI ionization based product detection.[21] As relative EI ionization cross sections are easily estimated, an accurate branching ratio could be derived: $\frac{CH_3+N_3}{CH_3N+N_2} = \frac{1.7\% \pm 0.4\%}{98.3\% \pm 0.4\%}$. Product translational energy distributions derived from the radical channel as well as their angular anisotropy parameters were energetically consistent with the cyclic-N_3 formation. We also identified a cyclic-N_3 formation through inspection of the translational energy release in the secondary dissociation of N_3 radicals.

$$N_3 \rightarrow N_2 + N(^2D). \tag{3}$$
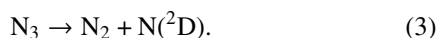
We concluded that cyclic-N_3 is the main 193-nm photoproduct in reaction (1). Furthermore, it was seen that, as desired, the fraction of cyclic-N_3 that underwent secondary dissociation was reduced in comparison to ClN_3.

The dominant molecular channel [reaction (2)] was complicated by several secondary, collision-free dissociation channels:

$$CH_3N \rightarrow CH_2NH, \tag{4}$$

$$CH_2NH \rightarrow HNC + H_2, \tag{5}$$

$$CH_2NH \rightarrow CH_2N + H, \tag{6}$$

$$CH_2N \rightarrow HCN + H. \tag{7}$$

Despite this complexity, reactions (4)–(7) were all clearly identified and characterized.

These two studies of CH_3N_3 clearly show that the branching between reactions (1) and (2) is wavelength dependent. In this work, we extend the previous studies at 248 and 193 nm. Specifically, we report observations of the elementary dissociation pathways and the energy release in methyl azide photodissociation at 157 nm using VUV-photoionization-based PTS experiments. The results are similar to the photodissociation dynamics at 193 nm; however, no linear N_3 was detected at this wavelength whatsoever. This is similar to the results obtained in a photodissociation study of ClN_3 at 157 nm.[13] Our results also allow us to derive a product branching ratio $\frac{\Phi_{CH_3-N_3}}{\Phi_{CH_3N-N_2}} = \frac{2.3\% \pm 0.6\%}{97.7\% \pm 0.6\%}$.

EXPERIMENTS

The experiments were carried out at the Chemical Dynamics Beamline 21 A of the National Synchrotron Radiation Research Center (NSRRC) in Hsinchu, Taiwan. A complete description of the apparatus used in this study has been previously published[22] and only the relevant details specific to this experiment are given here. The procedure to synthesize methyl azide has also been reported.[23,24] A mixture of 10% CH_3N_3 in Ne was prepared and stored in a stainless steel container and then used to form a supersonically cooled molecular beam by expanding into vacuum through a pulsed valve (Even-Lavie valve) with a backing pressure entering the source

chamber at ~1000 Torr. Cluster formation in the molecular beam was avoided by using a pulsed valve at temperatures slightly above 110 °C. The photofragmentation machine uses a rotating source chamber with a fixed detector. The molecular beam intersected an unpolarized, 157 nm excimer laser beam at right angles. The laser produced a 4–7 mJ/pulse and was shaped (3×8 mm² cross-section) with a focusing lens so that the short distance was along the time-of-flight (TOF) direction. The laser power was controlled to ensure that the TOF spectra were not the result of multiphoton processes. The neutral photofragments traveled 10.05 cm through two separate differentially pumped chambers prior to ionization by a beam of synchrotron radiation (1-mm spot size), which crossed at a right angle to the TOF axis in an ultrahigh vacuum chamber. The photo-ions were mass-selected by a quadrupole mass filter (QMF) before reaching a Daly-style detector for ion counting. The ion flight-times (from the ion source to the Daly detector) were determined independently and could be modeled with a simple formula, $\tau_{ion} = \alpha \cdot \sqrt{m}$, where $\alpha = 5.4$ μs amu$^{-1/2}$.

We measured the TOF spectra at all mass-to-charge ratios (m/z) where product signal could be detected: (m/z) = +14(N^+, CH_2^+), +15(CH_3^+), +27(HCN^+, HNC^+), +28(N_2^+, CH_2N^+), +29(CH_3N^+, CH_2NH^+), and +42(N_3^+) at laboratory angles, $\Theta_{lab} = 20°–60°$, in steps of 10°. Each TOF spectrum was averaged over a large number (3000–300 000) of laser shots.

We carried out experiments at various photoionization energies ($6.3 < h\nu_{synch} < 16.8$ eV) by changing the gap of the U9 undulator. The synchrotron photon energy spread exhibited a ~4% full width at half maximum (FWHM). Higher undulator harmonics were suppressed by an inert gas (Kr, Ne, or Ar) in a gas cell in a design similar to that described by Suits *et al.*[25]

In a separate set of experiments, we recorded the TOF spectra for m/z = +28 and m/z = +42 fragments in the energy ranges of 6.3–16.8 eV and 9.2–12.6 eV, respectively, in 0.20 eV steps at $\Theta_{lab} = 40°$ or 60°. The photo-fragments detected at m/z = +42 allowed us to measure the photoionization threshold for cyclic-N_3. The ion signal in each experiment was normalized to the laser power and the number of laser shots. The VUV intensity remained constant during all the experiments.

A forward convolution fitting approach was performed to analyze our data. We used the computer program PHOTRAN[26] to analyze primary dissociations and the program ANAL-MAX[27] to model secondary dissociation. Both programs simulate the TOF spectra based on a user input center-of-mass translational energy distribution, $P(E_T)$, which is adjusted iteratively until a satisfactory fit to the experimental data is obtained. For all our data analysis, an anisotropy parameter $\beta = 0$ was employed, which corresponds to an isotropic distribution due to the use of unpolarized light during the photolysis experiments.

RESULTS

Although mechanistically complex, the various photochemical channels of methyl azide are easily disentangled

TABLE I. Observed ion signals and their assignments to specific photochemical channels.

m/z[a]	Ion/neutral[b]	Primary channel	Secondary channel	$h\nu_{synch}$ (eV)[c]
14	N^+/N	(1)[d]	(3)	12.6
14	CH_2^+/CH_3	(1)	NA	11.7
15	CH_3^+/CH_3	(1)	NA	10.8
27	HNC^+/HNC	(2)	(5)	15.1
27	HCN^+/HCN	(2)	(4)-(6)-(7)	15.1
28	CH_2N^+/CH_2NH	(2)	NA	7.0–16.8
28	CH_2N^+/CH_2N	(2)	(6)	11.3–16.8
28	N_2^+/N_2	(1)	(3)	15.7–16.8
28	N_2^+/N_2	(2)	NA	15.7–16.8
29	CH_2NH^+/CH_2NH	(2)	NA	13.1
42	N_3^+/N_3	(1)	NA	11.7

[a]Observed mass to charge ratio.
[b]Detected ion and the neutral from which it originated.
[c]Synchrotron radiation tuned considering the ionization energy of the fragment analyzed.
[d]See text for an explanation of the reaction channel number.

with PTS, as has been previously demonstrated.[18,20,21] Our ability to discriminate by time-of-flight (TOF), detected mass-to-charge ratio, and the synchrotron photon energy, $h\nu_{synch}$, allows us to selectively look at all the products, essentially one by one. This greatly simplifies the assignment of the ion
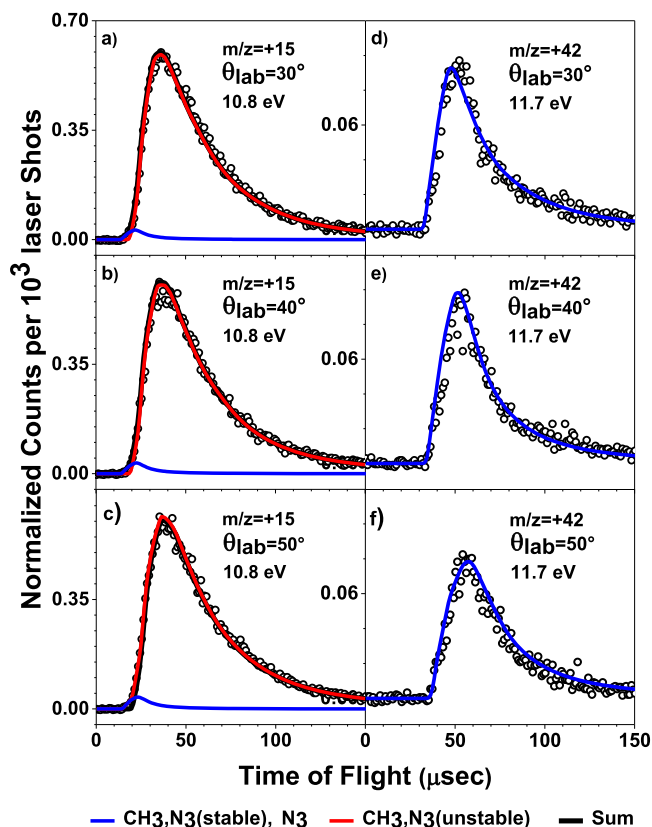
signal to its neutral photofragment. The various PTS experiments carried out in this work are summarized in Table I. The results allow us to unambiguously determine the collision-free photochemical decomposition mechanism—reactions (1)–(7) above.

TOF data are described in detail now. Figures 1(a)–1(c) show the TOF spectra of m/z = +15(CH_3^+) at $h\nu_{synch}$ = 10.8 eV and Figs. 1(d)–1(f) show m/z = +42(N_3^+) at $h\nu_{synch}$ = 11.7 eV. The data are represented by open circles. The solid lines are fits to the data, which are derived from the photochemical mechanism and derived energy release functions and will be described later. Both measured fragments can be attributed to the radical channel, reaction (1). The blue curves in these figures indicate momentum matched products. The red curve in Figs. 1(a)–1(c) come from methyl radicals whose momentum matched the N_3 photofragments decomposed before detection.

Secondary dissociation of N_3—reaction (3)—was observed in the TOF spectra at m/z = +14(N^+) and m/z = +28(N_2^+). The TOF spectra of m/z = +14 at 12.6 eV—Figs. 2(a) and 2(b)—show a single peak, which is associated with the N-atom formation in reaction (3). Surprisingly, we also observe the TOF signal at $h\nu_{synch}$ = 11.7 eV—Figs. 2(c) and 2(d). We attribute this minor signal to CH_2^+ formed via dissociative ionization from highly internally excited CH_3 fragments, as will be further explained below. Molecular nitrogen produced in reactions (2) and (3) was observed at m/z = +28 TOF spectra with $h\nu_{synch}$ = 16.5 eV — Figs. 3(a)–3(c). These spectra also exhibit other contributions to the m/z = +28 signal, indicating that species other than N_2 are present. In light of this, we investigated processes resulting from reactions (1)

FIG. 1. TOF spectra of m/z = +15 (a)-(c) and m/z = +42 (d)-(f) at laboratory detection angles Θ_{lab} = 30°-50°. The experimental data are shown as open circles. The blue lines represent the forward convolution simulation of the data using the P(E_T) distribution for reaction (1), shown in Fig. 6. The red lines represent a simulation of the methyl radical TOF and do not appear in the N_3 radical TOF as they are formed with so much internal energy that they dissociate before detection [reaction (3)]. Both fits were created using PHOTRAN.
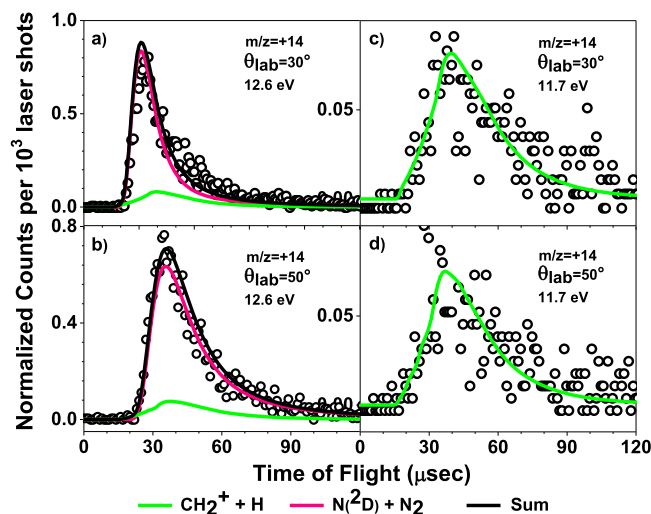

FIG. 2. TOF spectra of m/z = +14 recorded at (a) and (b) 12.6 eV and (c) and (d) 11.7 eV ionization photons, at laboratory detection angles Θ_{lab} = 30° and 50°. The experimental data are shown as open circles. In all spectra, the solid pink and green lines are the prediction of the ANALMAX secondary dissociation analysis program. The fit obtained over the m/z = +14 data at 11.7 eV is attributed to methyl radical that is detected after dissociative ionization $CH_3^+ \rightarrow CH_2^+ + H$ [reaction (10)]. This fit was obtained using a translational energy distribution with a maximum secondary energy release near zero kcal/mol. The solid pink fits obtained over the m/z = +14 data at 12.6 eV were derived using the translational secondary energy release in Fig. 8, which shows an average $\bar{E}_{Tmax} \sim$ 8.5 kcal/mol. This shows that the dissociation $N_2 + N(^2D)$ [reaction (3)] occurs.
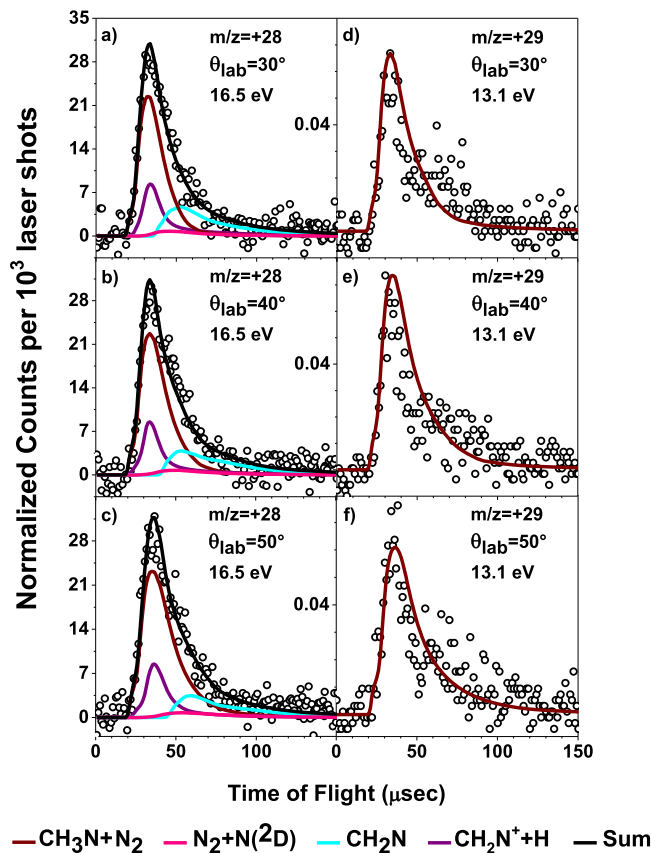
FIG. 3. TOF spectra of m/z = +28 (a)-(c) and m/z = +29 (d)-(f) at laboratory detection angles, Θ_{lab} = 30°-50°, in steps of 10°. The experimental data are shown as open circles. The brown lines represent the contributions from the molecular elimination channel [reaction (2)]. These were obtained from PHOTRAN and created using the primary $P_{CH3N}(E_T)$ distribution shown in Fig. 9. In the m/z = +28 TOF spectra, the purple and light blue lines represent the contribution of the dissociative ionization $CH_2NH^+ \rightarrow CH_2N^+ + H$ [reaction (14)] and the secondary dissociation channel [reaction (6)] from CH_3N fragments momentum matched to N_2 molecules [reaction (2)], respectively to the total signal. Both fits were also obtained using the total $P(E_T)$ translational energy distribution of CH_3N (Fig. 9) as the primary energy release and translational energy distributions with a secondary energy release near zero kcal/mol [Figs. 10(a) and 10(b)]. The pink lines represent secondary dissociation resulting from the N_3 molecules, $N_3 \rightarrow N_2 + N(^2D)$, formed after C–N rupture [reaction (1)]. This fit emerged using the secondary $P_N(E_{2T})$ distribution given in Fig. 8. The solid purple, light blue, and pink lines in the experimental data were constructed using ANALMAX.

and (2) involving a possible formation of HCNH, H_2CN, or N_2 by varying $h\nu_{synch}$.

Identification of these m/z = +28 fragments was carried out collecting the TOF data in the range of photon energies: 6.3–16.8 eV, at Θ_{lab} = 40°. See the supplementary material. This energy range was chosen by considering the ionization energies (IEs) of HCNH (IE = 7.0 eV[28]), H_2CN (IE = 10.43 eV,[29] 10.8 eV[28]), and N_2 (IE = 15.581 eV[30]). As expected, the m/z = +28 TOF data recorded showed a strong dependence on $h\nu_{synch}$. For example, at lower energies ($h\nu_{synch}$ = 7.0–10.4 eV) we found a single peak centered at 33 μs (Fig. S1 of the supplementary material) in contrast to the signal at $h\nu_{synch}$ = 11.3–14.9 eV, more intense and evidently with a late contribution (Fig. S2). Such a contribution remains detected at higher photoionization energies ($h\nu_{synch}$ = 15.7–16.8 eV), even when the signal recorded showed a dramatic increase (Fig. S3).
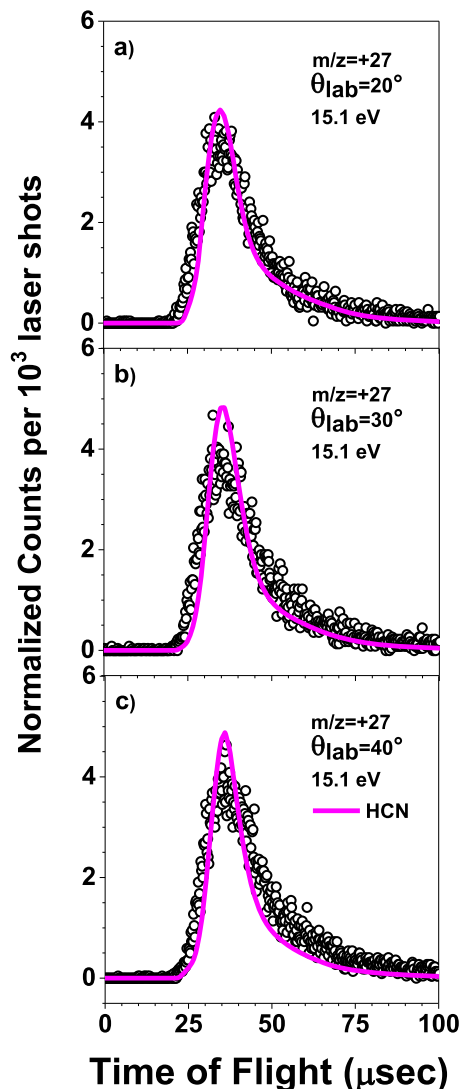

FIG. 4. TOF spectra of m/z = +27 with 15.1 eV ionization photons and laboratory detection angles, Θ_{lab}, of (a) 20°, (b) 30°, and (c) 40°. The experimental data are shown as open circles. In all spectra, the solid magenta lines are the fit from ANALMAX program using the translational energy distribution shown in Fig. 10(c).

For m/z = +29 (CH_3N^+, CH_2NH^+), TOF spectra were obtained at $h\nu_{synch}$ = 13.1 eV (Figs. 3(d)–3(f)), resulting from the primary dissociation in the molecular elimination channel [reaction (2)]. At 13.1 eV, only a single peak is detected at arrival times ~21–23 μs.

Finally, m/z = +27 (HCN^+, HNC^+) TOF spectra were recorded at $h\nu_{synch}$ = 15.1 eV (Figs. 4(a)–4(c)). They comprise a single peak at arrival times ~23 μs and are comparable to those detected in our previous works.[18,21] Analysis of all these spectra is considered extensively in the section titled "Discussion."

DISCUSSION

The energetics—zero-Kelvin enthalpies—for all possible photodissociation products of CH_3N_3 at 157 nm are shown in Fig. 5.[9,31] This diagram will be helpful to interpret the translational energy distributions $P(E_T)$, obtained from fits to the TOF data. The horizontal dashed black line indicates
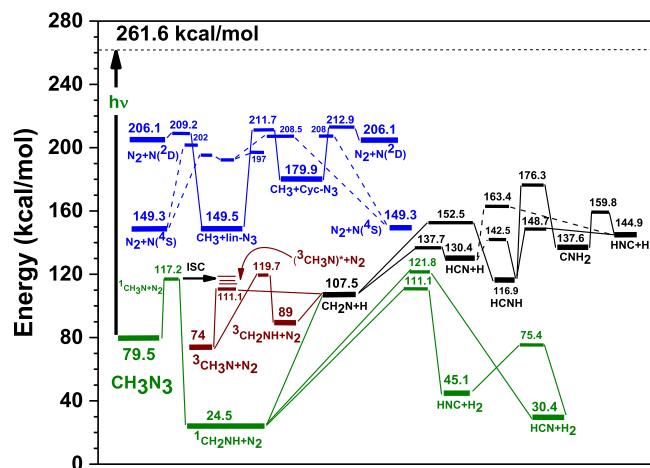
FIG. 5. Energy diagram for the primary and secondary dissociation pathways of methyl azide (CH_3N_3), constructed from Refs. 9 and 31. The dissociation pathways associated with the $CH_3 + N_3$ channel are shown as blue lines; those to the $CH_3N + N_2$ channel are presented as green (CH_2NH dissociation pathways), brown ($^3CH_3N$ isomers), and black lines (CH_2N isomers). "hν" on the solid vertical arrow indicates a single 157-nm photon (182.1 kcal/mol).

the available energy when methyl azide absorbs a single 157 nm photon. This section is organized as follows. First, an analysis of the primary and secondary photodissociation processes of the radical channel [reaction (1)] involving the fragments m/z = +15, +42, +28, and +14 is offered. Here, we show evidence of photoproduction of cyclic-N_3. Next, we discuss the results concerning the molecular channel [reaction (2)] and its subsequent dissociation pathways using data obtained at m/z = +29, +28, and +27. In this channel, several species were identified, including CH_2NH, CH_2N, HCN, and HNC.

The radical channel, $CH_3 + N_3$, and observation of cyclic-N_3

The center-of-mass (COM) translational energy distributions, referred to as $P(E_T)$, are derived from experimental TOF spectra. Without secondary dissociation of the primary products, $P(E_T)$ can be derived from the TOF of either of the photo-fragments of reaction (1) as their relative velocities are constrained by the conservation of linear momentum.

Figure 5 shows clearly, however, that many secondary dissociation processes are energetically allowed. To analyze the data of Fig. 1 (TOF spectra from the primary products of reaction (1), we decompose the $P(E_T)$ into two parts, $P_{CH3,N3(stable)}(E_T) \equiv P_{N3}(E_T)$, which describes the COM translational energy release leading to stable N_3 products, and $P_{CH3,N3(unstable)}(E_T)$, which is needed to describe the COM translational energy release of CH_3 whose momentum-matched N_3 product partners dissociated before they were detected in the experiment. $P_{CH3,N3(stable)}(E_T)$ and $P_{N3}(E_T)$ are shown as blue curves in Fig. 6 and are necessarily slanted to higher kinetic energy than $P_{CH3,N3(unstable)}(E_T)$, shown as a red curve in Fig. 6. By comparing the areas under $P_{CH3,N3(stable)}(E_T)$ and $P_{CH3,N3(unstable)}(E_T)$, we find that only about 5% of the N_3 fragments produced in the photolysis survive and do not undergo secondary dissociation.

Referring to Fig. 6, we may interpret these results. The available energy to form linear N_3, $E_{ava}^{lin} = 112.1$ kcal/mol, in reaction (1) is the difference between one 157 nm-photon ($h\nu_{photolysis} = 182.1$ kcal/mol) and the C–N bond energy of methyl azide, $D_0(CH_3-N_3) = 70$ kcal/mol.[32] This is the maximum translational energy release expected if CH_3 and linear-N_3 were formed with no internal energy (solid drop-down line marked as "A" in Fig. 6). Clearly no such large energy release is observed. In contrast, the available energy for the cyclic-N_3 formation, $E_{ava}^{cyc} = 81.8$ kcal/mol, is reduced by the cyclization energy of N_3 (30.3 kcal/mol[9]) (vertical line marked as "B" in Fig. 6). This corresponds closely to the maximum observed COM translational energy release. We also note that the maximum translational energy release of the $P_{CH3,N3(unstable)}(E_T)$, that is, the energy release for the part of reaction (1) where the N_3 subsequently dissociates is 46 kcal/mol, a value that coincides well with the predicted spin-allowed energy barrier for the dissociation of cyclic-N_3—$N_2 + N(^2D)$, reaction (3)—marked as "F."

Alternatively, we may use our derived $P(E_T)$ to obtain heat of formation for cyclic-N_3, $\Delta_fH°(cyclic-N_3)$, which has been previously reported as part of the study of ClN_3 photochemistry at 157 nm, $\Delta_fH°(cyclic-N_3) = 140.9 \pm 3.5$ kcal/mol.[13] Following a similar analysis, we obtain as result from our data

$$\Delta_fH°(cyclic-N_3) = h\nu_{photolysis} + \Delta_fH°(CH_3N_3) - \Delta_fH°(CH_3) - E_{T,m/z=+42}^{max}$$
$$= (182.1 + 75.9 - 35.85 \pm 0.07 - 82 \pm 2)\ kcal/mol$$
$$= 140.15 \pm 2\ kcal/mol. \tag{8}$$

Here, values for $\Delta_fH°(CH_3N_3)$ and $\Delta_fH°(CH_3)$ were obtained from Refs. 33 and 34, respectively. To further confirm this assignment, additional experiments were carried out to determine the dependence of the m/z = +42 signal on $h\nu_{synch}$. Figure 7 shows the TOF-signal integrated vs $h\nu_{synch}$, seen as solid blue circles. All the integrated intensities were normalized to the laser power and the number of laser shots. The intersection of the two black lines indicates

the IE threshold derived from this work (∼10.65 eV) consistent with previous theoretical[15] and experimental[12,18] reports.

The sum total of this analysis gives rather strong evidence that cyclic-N_3 is the dominant product of reaction (1) at 157 nm. The dynamical reasons for this are not clear. It could be that the potential energy surface involved simply leads more easily to the strongly N–N–N bent configurations needed to produce
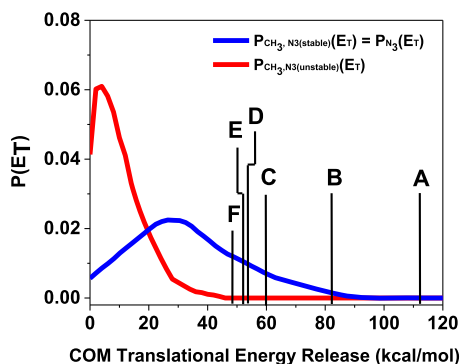
FIG. 6. Center-of-mass (COM) translational energy release distributions [$P(E_T)$], used to simulate the m/z = +15 and m/z = +42 TOF data in Fig. 1. All $P(E_T)$ distributions are the result of the forward convolution analysis performed over the data obtained at scattering angles, $\Theta_{lab} = 30°$-$50°$. The $P_{CH_3,N_3(stable)}$ $(E_T) \equiv P_{N3}(E_T)$ distribution, shown as blue line, was created after fitting those contributions assigned to the cyclic-N_3 forming channel [reaction (1)], whilst the $P_{CH_3,N_3(unstable)}$ (E_T) (red line) resulted from the forward convolution analysis performed over the contribution attributed to the fragments of m/z = +15 (CH_3^+) whose N_3 fragments lead to secondary dissociation [reaction (3)]. Solid drop-down lines indicate the maximum translational energy for the CH_3 + linear-N_3 (marked as "A") and CH_3 + cyclic-N_3 ("B") channels, the energy of the highest energy doublet/quarter (D/Q) surface seam of crossing for linear N_3 (indicated as "C"), the energy of the lowest energy doublet/quarter (D/Q) surface seam of crossing for cyclic-N_3 ("D"), and the energies of the barrier to dissociation for linear N_3 ("E") and for cyclic-N_3 ("F"), following photolysis of CH_3N_3 at 157 nm. The excellent agreement with the predictions described for cyclic-N_3 provides proof of exclusive production of this species under the experimental conditions indicated in the text.

the cyclic isomer. An alternative dynamical explanation could involve a higher propensity for linear N_3 to undergo secondary dissociation, compared to the cyclic isomer. We now take up the analysis of data from this work, which strongly suggests that the majority of secondary N_3 dissociation proceeds from the cyclic structure.

Secondary dissociation in the radical channel

In the following, we discuss the dissociation of energetic N_3 and CH_3 fragments. Our approach is to understand the formation of atomic Nitrogen in reaction (3) using the m/z

= +14 TOF data obtained at $h\nu_{synch}$ = 12.6 eV—Figs. 2(a) and 2(b). This analysis is complicated by the observation of the m/z = +14 signal for $h\nu_{synch}$ = 11.7 eV [Figs. 2(c) and 2(d)], which cannot result from the N-atom. We first dispose of this minor matter. CH_2 formation

$$CH_3 \rightarrow CH_2 + H \tag{9}$$

is not energetically accessible under our conditions. However, dissociative ionization of CH_3 is possible, if methyl radicals can be formed with large amounts of internal energy.

$$CH_3^+ \rightarrow CH2^+ + H. \tag{10}$$

Usually, tunable VUV-synchrotron photoionization reduces the importance of dissociative ionization. However, when the translational energies of the neutral products are low—large photoproduct internal energy—fragmentation following ionization can occur. The solid green lines of Fig. 2 are fully consistent with the data.

Having accounted for the small contribution of CH_3 dissociative ionization to the m/z = +14 data, we can quickly conclude that at $h\nu_{synch}$ = 12.6 eV $N(^2D)$ atoms are the major product of secondary N_3 dissociation [reaction (3); Figs. 2(a) and 2(b)], since under these energy conditions only this spin-allowed dissociation product of N_3 can be ionized, [IE(N^2D)] = 12.15 eV. We fit this secondary dissociation data as in previously reported work.[18,21] Briefly, one requires two translational energy distributions $P(E_T)$. The first is the $P(E_T)$ for the N_3 molecules that dissociate, $P_{N3}(E_T)$. This is used together with the COM translational energy release associated with reaction (3), $P_N(E_{2T})$ to calculate the observed laboratory frame TOF spectra (see Fig. 8).

One immediately realizes that the $P_N(E_{2T})$ distribution shows an average translational energy release, $\bar{E}_T$ ~ 8.5 kcal/mol, consistent with the predicted exit barrier (7 kcal/mol)[9] for cyclic-N_3 dissociation to $N(^2D)$ and N_2. This is markedly higher than the analogous barrier for linear N_3 dissociation. It also agrees with the $P_N(E_{2T})$ distribution derived from similar PTS experiments at 193 nm,[21] seen as
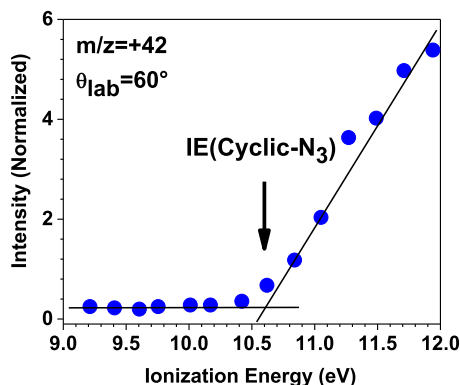

FIG. 7. Photoionization energy of the m/z = +42 TOF signal vs ionization photon energy. A normalization procedure of the integrated intensities at laboratory angle $\Theta_{lab} = 60°$ was carried out considering the laser power and number of laser shots. The solid arrow indicates the literature value (10.595 eV)[15] for the ionization energy (IE) of cyclic-N_3. The intersection of the two solid lines provides an estimation of the IE measured in this experiment at ~10.6 eV.

FIG. 8. Secondary translational energy release distribution obtained from the analysis of the m/z = +14 data of Figs. 2(a) and 2(b). This distribution, shown as solid-pink circles, describes the translational energy release of the process $N_3 \rightarrow N_2 + N(^2D)$, detected when the undulator gap produced VUV ionizing radiation at $h\nu_{synch}$ = 12.6 eV. This distribution was also used to simulate the portion of N_2 molecules detected in the m/z = +28 TOF spectra shown in Figs. 3(a)–3(c) and Fig. S3 of the supplementary material. For comparison purposes, the same distribution obtained at 193 nm[21] was included as the dashed-pink line.

a dashed line in Fig. 8. This result provides additional support to our interpretation that cyclic-N_3 dissociates through a spin-allowed channel.
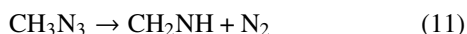
Following this line of reasoning, an analysis of the N_2 molecules produced in reaction (3) is now required. However, m/z = +28 TOF spectra recorded at different $h\nu_{synch}$ values [Figs. 3(a)–3(c)] clearly suggest a complex photochemistry involving a number of contributions to the m/z = +28 ion signal.

This leads us to analyze the N_2 products of reaction (3) along with these other contributions. As discussed in the section titled "Molecular elimination channel, $CH_3N + N_2$: Primary dissociation," our observations indicate the presence of N_2 dissociated from N_3 [reaction (3)] and from the molecular channel [reaction (2)] along with CH_2N.

Molecular elimination channel, $CH_3N + N_2$: Primary dissociation

Figures 3(d)–3(f) shows the m/z = +29 TOF data obtained when the undulator gap produced photons at $h\nu_{synch}$ = 13.1 eV, thus allowing us to observe species as methanimine [IE(CH_2NH) = 9.97 eV[35]]. These TOF spectra are fit using the $P_{CH3N}(E_T)$ distribution, shown as a solid brown line in Fig. 9. This $P(E_T)$ comprises a single feature with an average translational energy release of $\bar{E}_T = 26$ kcal/mol and a maximum translational energy release $E_T^{max} = 122$ kcal/mol. Taking into account the energy diagram (Fig. 5), we clearly find that the CH_3N and N_2 fragments are "momentum matched," and given the small $\bar{E}_T$ for m/z = +29, a rapid isomerization $^1CH_3N \rightarrow CH_2NH$ [reaction (4)] follows once CH_3N is formed. This isomerization is attributed to the limited available energy appearing as translation in this fragment, as it has been seen in previous works at 248 nm[20] and 193 nm.[18,21]

A simple energetic analysis for the direct formation of methanimine [reaction (11)] can confirm this evidence. Under the current conditions of our experiment,

$$CH_3N_3 \rightarrow CH_2NH + N_2 \tag{11}$$

provides 237.1 kcal/mol of available energy, in comparison to 144.4 kcal/mol if reaction (2) is assumed. This implies that

the $\bar{E}_T$ represents only 11% of the available energy in reaction (11), whilst for reaction (2), it increases to 18%. The lowest ratio $\frac{E_T}{E_{ava}}$ clearly suggests that the direct formation of $CH_2NH + N_2$ would be rarer to observe than the molecular channel, followed by the isomerization to CH_2NH. Observations comparable to our results have been reported before and explained through invoking the soft product impulse approximation.[36]

We also note that the forward convolution fit from PHOTRAN is not perfect for all the fragments arriving at later times [Figs. 3(d)–3(f)]. We believe this corresponds to a small contribution of vibrationally excited molecules of the $^1CH_3N$ or $^1CH_2NH$ ionization, not fully resolved by the wavelength dependent photoionization. Also, attempts were carried out to fit possible contributions from reactions involving triplet species, such as $^3CH_3N$ and $^3CH_2NH$, but we found no evidence to this.

$P_{CH3N}(E_T)$ distribution was also useful to explain the m/z = +28 TOF data at $h\nu_{synch}$ = 16.5 eV [Figs. 3(a)–3(c)], through creating the identical distribution $P_{N2}(E_T)$. Under this condition, photons are capable of ionizing N_2, thus leading to the exploration of all possible contributions in the molecular elimination channel [reaction (2)]. In Figs. 3(a)–3(c), we note immediately not only that the $P_{N2}(E_T)$ distribution produces the largest contribution to the total m/z = +28 signal but also that other species are required to properly fit the data.

Secondary dissociation in the molecular elimination channel

We have already stated that the energy diagram in Fig. 5 suggests that a great variety of reaction pathways contribute to the m/z = +28 spectra, as those producing H_2CN, H_2NC, $HCNH$, and N_2 (eliminated through both the radical and molecular channels). To rule out if such species were produced in our experiment, we performed a photoionization energy dependence study of the m/z = +28 TOF signal. We varied the wavelength of the ionization synchrotron radiation in an energy range of 6.3–16.8 eV and recorded the TOF spectra in steps of $\sim$0.2 eV, at a laboratory angle $\Theta_{lab} = 40°$. A representative set of the fitted TOF spectra for m/z = +28 at $h\nu_{synch}$ = 16.5 eV is presented in Figs. 3(a)–3(c). Here, the fits emerged as a result of monitoring the evolution of the m/z = +28 TOF data in this energy range, as shown in the supplementary material (Figs. S1-S3). In each normalized TOF spectrum, we inspected for contributions, which were then resolved accordingly.

Our analysis of the molecular elimination channel is obscured by the initial observation of the m/z = +28 signal in the range $h\nu_{synch}$ = 7.0–10.4 eV (Fig. S1 of the supplementary material). HCNH, formed from the isomerization of CH_2N as a tertiary event,

$$CH_2N \rightarrow HCNH, \tag{12}$$

and similarly H_2NC from HCNH,

$$HCNH \rightarrow H_2NC, \tag{13}$$

cannot be associated with this signal. First, the linear isomer of HCNH is unlikely to undergo a transition from its neutral
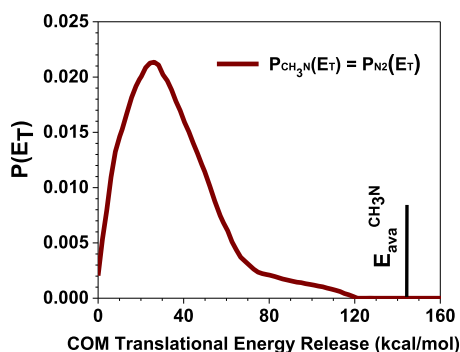

FIG. 9. Center-of-mass (COM) translational energy release distribution $P_{CH3N}(E_T)$, used to simulate the m/z = +29 TOF data shown in Figs. 3(d)–3(f). This distribution was also used to simulate the portion of N_2 molecules from reaction (2) ($CH_3N_3 \rightarrow CH_3N + N_2$) in the m/z = +28 TOF data at $h\nu_{synch}$ = 16.5 eV [Figs. 3(a)–3(c)], and in Fig. S3 of the supplementary material. The vertical line marked at E_T = 144.4 kcal/mol shows the theoretical maximum translational primary energy release for reaction (2).

ground to its bent ion state due to small FC-factors[29] and second, the experimental and theoretical determinations of the ionization energies for *trans*-HCNH, *cis*-HCNH, and H_2NC prevented us to explore the presence of these species here.[29] In order to explain the observations in this energy range, we fit our data using the forward convolution simulation provided by ANALMAX, considering the primary $P_{CH3N}(E_T)$ distribution (Fig. 9) to characterize the primary reaction [reaction (2)] and a near-zero kinetic energy release distribution [Fig. 10(a)] for a possible secondary dissociation. This result is seen in Fig. S1 as solid purple lines. Given that the CH_2NH fragments were formed with large internal energies inferred from the limited translational energy release shown in Fig. 9, we believe this observation corresponds to the dissociative ionization

$$CH_2NH^+ \rightarrow CH_2N^+ + H \tag{14}$$
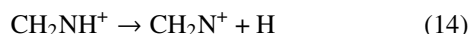
that remains important at all photoionization energies employed in this experiment, even when typically such a fragmentation is expected to be inhibited.
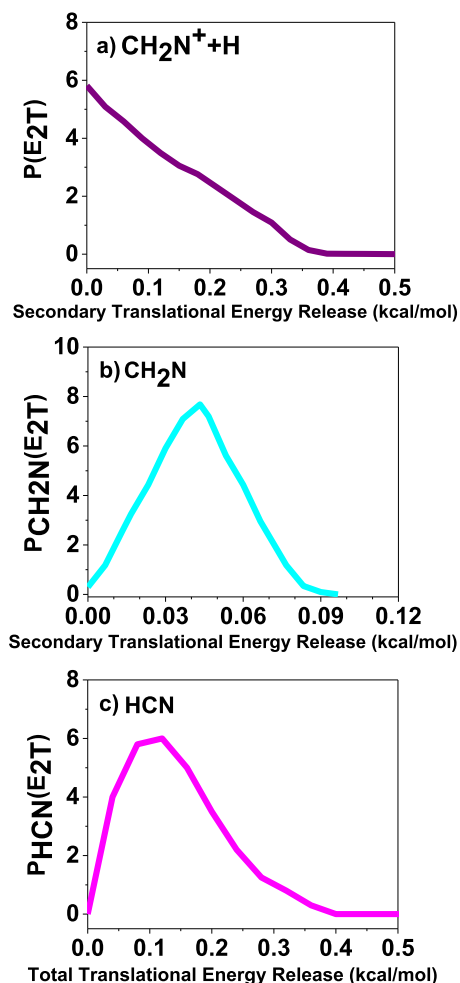

FIG. 10. Secondary translational energy distributions used to fit the TOF data of (a) m/z = +28(CH_2NH^+ + H) [seen as purple lines in Figs. 3(a)–3(c) and in Figs. S1–S3 of the supplementary material], (b) m/z = +28(CH_2N^+) [seen as light blue lines in Figs. 3(a)–3(c) and Figs. S2 and S3], and (c) m/z = +27(HCN^+/HNC^+) [seen as magenta lines in Figs. 4(a)–4(c)]. All these secondary translational energy distributions were determined using ANALMAX.

Recall that the m/z = +28 TOF spectra in $h\nu_{synch}$ = 11.3–14.9 eV (Fig. S2 of the supplementary material) progressively shows a second contribution at later times. The fast signal is immediately assigned to the CH_2N^+ formation via reaction (14), by using the same procedure as in $h\nu_{synch}$ = 7.0–10.4 eV. Here, we easily realize that any additional signal remains unrelated to the N_2 formation, given that the ionizing synchrotron radiation was not sufficient to ionize such molecules. Therefore, a fitting procedure for the slow contribution was carried out considering the CH_2N formation from neutral methanimine [CH_2NH, reaction (6)] with H-atom loss, as it has been reported previously.[18,21] To fit the data, we use the $P_{CH3N}(E_T)$ distribution (Fig. 9) for the primary release and the $P_{CH2N}(E_{2T})$ distribution [shown as solid light blue line in Fig. 10(b)] for the secondary release. As a result, the maximum energy release for the secondary distribution falls to zero at ~0.06 kcal/mol, consistent with the formation of CH_2N through a simple bond rupture with an H-atom release. Given all this, we can clearly distinguish between the daughter ion and the secondary product of CH_2N in two different ranges of photoionization energy.

An analysis of the TOF data in $h\nu_{synch}$ = 15.7–16.8 eV is followed now. Here, we estimate contributions of N_2 from reactions (2) (N_2 + CH_3N) and (3) [N_2 + N(^{2}D)] to the total m/z = +28 signal, by considering those already found from reactions (6) and (14). These contributions are shown as light blue and purple lines in Figs. 3(a)–3(c) and Fig. S3 of the supplementary material, correspondingly. To simulate the contribution from reaction (2), we used the translational energy distribution $P_{N2}(E_T)$ into the same TOF data, strongly suggesting that the formation of N_2 is dominant through this molecular channel. Similarly, we simulate the contribution of N_2 secondarily dissociated from N_3 fragments [reaction (3)] using the energy distribution $P_N(E_{2T})$ over the same data (shown as solid pink lines), resulting in a small contribution that is considered to fully resolve the m/z = +28 TOF signal.

Finally, we study the m/z = +27 photofragments, recorded at $h\nu_{synch}$ = 15.1 eV [Figs. 4(a)–4(c)], in which the presence of HCN (or HNC) [IE(HCN) = 11.5 eV[37] (theoretical), <12.07 eV[38] (experimental)] and HNC [IE(HNC) = 13.0 eV[37] (theoretical), 13.607 ± 0.002 eV[39] (experimental)] can be detected. As shown in the energy diagram (Fig. 5), CH_2NH can produce HCN or HNC having H_2 as a counter-fragment, or after two subsequent H-atom departures, HCN is formed and then isomerized to HNC. We noted the similar shape of the m/z = +27 TOF spectra with those in our previous work[21] in which the signal was attributed to reaction (7) and described as a tertiary process. Consequently, we use ANALMAX to evaluate this possibility, in which the simulated tertiary processes is treated as a secondary step, assuming that a secondary translational energy distribution $P(E_{2T})$ provides a maximum near zero. Our best fits (seen as solid magenta lines in Fig. 4) reveal that reaction (7) is the most likely process in our experiment. Such a fitting was created after using the distribution $P_{CH3N}(E_T)$ (Fig. 9) for the primary translational energy release and $P_{HCN}(E_{2T})$ [Fig. 10(c)] for the secondary release. The $P_{HCN}(_{2T})$ distribution obtained shows a maximum secondary energy release of ~0.35 kcal/mol,

TABLE II. Estimated product branching ratio R of $CH_3 + N_3$ versus $CH_3N + N_2$ for laboratory angles, $\Theta_{lab} = 20°-60°$.

Θ_{lab}	$\dfrac{\left(N_{CH_3^+, \text{ reaction 1}}/N_{N_2^+, \text{ reaction 2}}\right)_{157 \text{ nm}}}{\left(N_{CH_3^+, \text{ reaction 1}}/N_{N_2^+, \text{ reaction 2}}\right)_{193 \text{ nm}}}$	R
20	1.38	0.024
30	1.32	0.023
40	1.28	0.022
50	1.29	0.022
60	1.19	0.021

agreeing well with this assumption. The excellent similarity between the experimental results at 197 and 157 nm suggests that the m/z = +27 fragments may have the same energetic origin.

Branching ratios of detected dissociation channels

An accurate product branching ratio can be obtained for the radical [reaction (1)] and molecular channels [reaction (2)] if relative photoionization cross-sections are known for the observed products. However, most of these cross-sections have remained undetermined since we carried out our previous experiments using synchrotron radiation.[18] Fortunately, if we compare the TOF signal levels for the nonreactive scattering of CH_3 and N_2 [reaction (2)], $N_{CH_3^+, \text{ reaction 1}}$ and $N_{N_2^+, \text{ reaction 2}}$, from our current experiments with available from electron impact ionization data,[21] we can extract easily a global branching ratio **R** for $CH_3 + N_3$ versus $CH_3N + N_2$ within our experimental uncertainty. The global branching ratio was obtained after following an appropriate normalization (VUV intensity, laser power, and the number of laser shots) of the data at a few different laboratory angles ($\Theta_{lab} = 20°$-$60°$), in both the photoionization and electron impact data. In the experiments based on electron impact ionization, the cross sections for the primary products were estimated[40] using additivity rules, resulting in the cross sections of 3.7×10^{-16} cm^2 for CH_3 and 2.6×10^{-16} cm^2 for N_2. Branching ratios for CH_3 versus N_2 [reaction (2)] for the several laboratory angles considered in this work are presented in Table II, using the photoionization energies of 11.7 eV for CH_3 and 16.5 eV for N_2. From the table, a global product branching ratio for the C–N and N–N ruptures in CH_3N_3 of $\frac{\Phi_{CH_3 - N_3}}{\Phi_{CH_3N - N_2}} = \frac{2.3\% \pm 0.6\%}{97.7\% \pm 0.6\%}$ is obtained. Considering that only ~5% of the N_3 fragments present in reaction (1) fail to undergo secondary dissociation, we conclude that ~0.12% of these molecules produced during the photolysis of CH_3N_3 at 157 nm are cyclic-N_3.

CONCLUSION

Methyl azide (CH_3N_3) has been photodissociated at 157 nm under collision-free conditions, and the resulting photoproducts (N_3, CH_2NH, N_2, CH_2N, HCN/HNC, CH_3, CH_2, and N) have been detected using VUV synchrotron radiation-based photofragment translational spectroscopy. All the evidence obtained suggests exclusive production of the cyclic isomer of N_3, in contrast to previous work at other photolysis

wavelengths. At 157 nm, the C–N dissociation in CH_3N_3 that leads to the formation of this isomer is increased by ~35% with respect to the results obtained previously at 193 nm, thus obtaining a branching product ratio of $\frac{\Phi_{CH_3 - N_3}}{\Phi_{CH_3N - N_2}} = \frac{2.3\% \pm 0.6\%}{97.7\% \pm 0.6\%}$. This work also confirms the important experimental data associated with Cylic-N_3, including its heat of formation and ionization energy.

SUPPLEMENTARY MATERIAL

See supplementary material for the m/z = +28 TOF signal in the photon energy range 7.0–16.8 eV.

[1]N. Hansen and A. M. Wodtke, J. Phys. Chem. A **107**(49), 10608–10614 (2003).
[2]N. Hansen, A. M. Wodtke, S. J. Goncher, J. C. Robinson, N. E. Sveum, and D. M. Neumark, J. Chem. Phys. **123**(10), 104305 (2005).
[3]A. Vij, J. G. Pavlovich, W. W. Wilson, V. Vij, and K. O. Christe, Angew. Chem., Int. Ed. **41**(16), 3051–3054 (2002).
[4]H. Ostmark, S. Wallin, T. Brinck, P. Carlqvist, R. Claridge, E. Hedlund, and L. Yudina, Chem. Phys. Lett. **379**(5-6), 539–546 (2003).
[5]P. C. Samartzis and A. M. Wodtke, Int. Rev. Phys. Chem. **25**(4), 527–552 (2006).
[6]M. Bittererova, H. Ostmark, and T. Brinck, J. Chem. Phys. **116**(22), 9740–9748 (2002).
[7]A. Friedmann, A. M. Soliva, S. A. Nizkorodov, E. J. Bieske, and J. P. Maier, J. Phys. Chem. **98**, 8896 (1994).
[8]D. Babikov, V. A. Mozhayskiy, and A. I. Krylov, J. Chem. Phys. **125**(8), 084306 (2006).
[9]P. Zhang, K. Morokuma, and A. M. Wodtke, J. Chem. Phys. **122**(1), 014106 (2005).
[10]S. J. Goncher, N. E. Sveum, D. T. Moore, N. D. Bartlett, and D. M. Neumark, J. Chem. Phys. **125**(22), 224304 (2006).
[11]A. M. Wodtke, N. Hansen, J. C. Robinson, N. E. Sveum, S. J. Goncher, and D. M. Neumark, Chem. Phys. Lett. **391**(4-6), 334–337 (2004).
[12]P. C. Samartzis, J. J. M. Lin, T. T. Ching, C. Chaudhuri, Y. T. Lee, S. H. Lee, and A. M. Wodtke, J. Chem. Phys. **123**(5), 051101 (2005).
[13]P. C. Samartzis, J. J. M. Lin, T. T. Ching, C. Chaudhuri, S. H. Lee, and A. M. Wodtke, J. Chem. Phys. **126**(4), 041101 (2007).
[14]P. C. Samartzis, N. Hansen, and A. M. Wodtke, Phys. Chem. Chem. Phys. **8**(25), 2958–2963 (2006).
[15]V. A. Mozhayskiy, D. Babikov, and A. I. Krylov, J. Chem. Phys. **124**, 224309 (2006).
[16]J. Y. Zhang, K. J. Yuan, Y. Chen, S. A. Harich, X. Y. Wang, X. M. Yang, and A. M. Wodtke, Chin. J. Chem. Phys. **20**(4), 345–351 (2007).
[17]J. Y. Zhang, P. Zhang, Y. Chen, K. J. Yuan, S. A. Harich, X. Y. Wang, Z. Wang, X. M. Yang, K. Morokuma, and A. M. Wodtke, Phys. Chem. Chem. Phys. **8**(14), 1690–1696 (2006).
[18]C. Larson, Y. Ji, P. C. Samartzis, A. Quinto-Hernandez, J. J. M. Lin, T. T. Ching, C. Chaudhuri, S. H. Lee, and A. M. Wodtke, J. Phys. Chem. A **112**(6), 1105–1111 (2008).
[19]P. C. Samartzis and A. M. Wodtke, Phys. Chem. Chem. Phys. **9**(24), 3054–3066 (2007).
[20]C. Larson, Y. Y. Ji, P. Samartzis, A. M. Wodtke, S. H. Lee, J. J. M. Lin, C. Chaudhuri, and T. T. Ching, J. Chem. Phys. **125**(13), 133302 (2006).
[21]A. Quinto-Hernandez, J. Doehla, W. T. Huang, C. Y. Lien, W. Y. Lin, J. J. M. Lin, and A. M. Wodtke, J. Phys. Chem. A **116**(19), 4695–4704 (2012).
[22]J. J. Lin, Y. Chen, Y. Y. Lee, Y. T. Lee, and X. M. Yang, Chem. Phys. Lett. **361**, 374–382 (2002).

[23] M. Khlifi, P. Paillous, P. Bruston, F. Raulin, and J. C. Guillemin, Icarus **124**(1), 318–328 (1996).

[24] A. T. Roos, H. Gilman, and N. J. Beaber, Org. Syntheses **1**, 145–147 (1932).

[25] A. G. Suits, P. Heimann, X. M. Yang, M. Evans, C. W. Hsu, K. T. Lu, Y. T. Lee, and A. H. Kung, Rev. Sci. Instrum. **66**(10), 4841–4844 (1995).

[26] S. A. Harich, PHOTRAN (2003).

[27] A. M. Wodtke, "Very high resolution Photofragmentation-Translational Spectroscopy," Ph.D. dissertation (University of California, Berkeley, 1986).

[28] F. L. Nesbitt, G. Marston, L. J. Stief, M. A. Wickramaaratchi, W. Tao, and R. B. Klemm, J. Phys. Chem. **95**(20), 7613–7617 (1991).

[29] F. Holzmeier, M. Lang, K. Hader, P. Hemberger, and I. Fischer, J. Chem. Phys. **138**(21), 214310 (2013).

[30] T. Trickl, E. F. Cromwell, Y. T. Lee, and A. H. Kung, J. Chem. Phys. **91**(10), 6006–6012 (1989).

[31] M. T. Nguyen, D. Sengupta, and T. K. Ha, J. Phys. Chem. **100**(16), 6499–6503 (1996).

[32] A. Quinto-Hernandez, Y. Y. Lee, T. P. Huang, W. C. Pan, R. A. Mata, and A. M. Wodtke, J. Phys. Chem. Lett. **2**, 2311–2315 (2011).

[33] K. E. Gutowski, R. D. Rogers, and D. A. Dixon, J. Phys. Chem. A **110**(42), 11890–11897 (2006).

[34] B. Ruscic, J. E. Boggs, A. Burcat, A. G. Csaszar, J. Demaison, R. Janoschek, J. M. L. Martin, M. L. Morton, M. J. Rossi, J. F. Stanton, P. G. Szalay, P. R. Westmoreland, F. Zabel, and T. Berces, J. Phys. Chem. Ref. Data **34**(2), 573–656 (2005).

[35] H. Bock and R. Dammel, Chem. Ber./Recl. **120**(12), 1961–1970 (1987).

[36] S. J. Riley and K. R. Wilson, Faraday Discuss. Chem. Soc. **53**, 132–146 (1972).

[37] D. Talbi, A. Le Padellec, and J. B. A. Mitchell, J. Phys. B: At., Mol. Opt. Phys. **33**(18), 3631–3646 (2000).

[38] S. Petrie, C. G. Freeman, M. Meotner, M. J. Mcewan, and E. E. Ferguson, J. Am. Chem. Soc. **112**(20), 7121–7126 (1990).

[39] C. Fridh and L. Asbrink, J. Electron Spectrosc. Relat. Phenom. **7**(2), 119–138 (1975).

[40] W. L. Fitch and A. D. Sauter, Anal. Chem. **55**(6), 832–835 (1983).